Results in Materials 17 (2023) 100360

Contents lists available at ScienceDirect

Results in Materials

journal homepage: www.sciencedirect.com/journal/results-in-materials

Investigation the temperature-dependent surface mechanical properties of PolyJet printed samples by cyclic indentation testing in a DMA system

Luca Kotrocz, Péter Bakonyi *

Department of Polymer Engineering, Faculty of Mechanical Engineering, Budapest University of Technology and Economics, 1111 Budapest, Műegyetem rakpart 3., Hungary

ARTICLE INFO

Keywords:
Cyclic
Indentation
Creep behavior
Relaxation behavior
Temperature dependence
Photopolymer
Additive manufacturing

ABSTRACT

Tools and products used in everyday life are regularly exposed to dynamic, cyclical stress. These stresses are particularly significant in the case of polymers, as their viscoelastic behavior means that creep can be considerable even at room temperature. Therefore, polymer components are often tested for maximum deformation rather than for maximum load-bearing capacity. Basic material testing methods are tensile, compression, and flexure tests, which are excellent for determining the material properties of the bulk material. However, in some cases, it is more appropriate to investigate surface mechanical properties. The ideal method for this is the depth-sensing indentation test. This method has been widely applied to polymers in the last ten years, but cyclic tests are rare, and creep is not considered in this type of indentation test. In the case of cyclical tests, temperature dependence is not fully examined, either. This paper presents the results of cyclic indentation tests on photopolymer specimens produced by additive manufacturing with the use of a dynamic mechanical analyzer with a unique indentation clamp. We performed the tests at three temperatures to investigate the influence of temperature on cyclic indentation tests. The test results show the variation of deformation between cycles and the significant effect of temperature.

1. Introduction

Thanks to the development of additive manufacturing (AM) technologies, products can be used as visual prototypes for design purposes and as functional products. One of the main applications of additive manufacturing is rapid tooling (RT). Additive manufactured tools can be used for injection molding mold inserts. These inserts are typically manufactured with three types of technology: selective laser sintering (SLS), stereolithography (SLA), or the PolyJet technology [1–3]. Injection molding is a discontinuous technology, and during production, there are great forces and thermal stresses [4]. For polymer injection molding tool inserts, these stresses are of particular importance, as polymers behave differently from metals.

Traditional material testing methods are available for testing polymers as well, i.e., tensile, compression, bending and shear tests, and twisting. All these can be combined with cyclic loading, or temperature dependence can be investigated in a heat chamber [5]. Several researchers have tested the mechanical properties of specimens produced with different AM technologies. For fused deposition modeling (FDM), Galeja et al. [6] tested the influence of infill shape and percentage. Szykiedabs and Credo [7] compared FDM and SLA using tensile tests. Sagias et al. [8] carried out more complex tests for of production parameters, such as layer thickness, placement, infill shape, and print strength. Miedzińska et al. [9] studied the strength properties of SLA at different strain rates. They also used the tensile test to describe yield strength, the elastic and plastic behavior and the brittleness of the material. Vidakis et al. [10] used tensile, flexural and micro-hardness (Vickers) tests, and thermal analysis to determine the mechanical parameters of their acrylonitrile-butadiene-styrene–zinc oxide (ABS-ZnO) nano- and microcomposites. Anderson [11] used tension, shear, and hardness (Shore D) tests on virgin and recycled polylactic acid (PLA) specimens. Hanon et al. [12] made a comprehensive series of tests on the effect of manufacturing parameters on the tensile strength of PLA specimens. Kundera and Kozior [13] determined the mechanical properties of glass fiber–reinforced polyamide manufactured by SLS. They used tensile and tribological tests. Ribeiro et al. [14] tested the thermal properties of SLA resin. The effect of orientation on the mechanical properties of PolyJet technology products [15] and fatigue properties [16] were also investigated. For shape-memory 3D printed test specimens, both thermal and cyclic tests are important [17,18].

These tests determine the mechanical properties of a material, but for

* Corresponding author.
E-mail addresses: kotroczl@pt.bme.hu (L. Kotrocz), bakonyi@pt.bme.hu (P. Bakonyi).

https://doi.org/10.1016/j.rinma.2022.100360
Received 26 July 2022; Received in revised form 15 December 2022; Accepted 21 December 2022
Available online 23 December 2022

Abbreviations

A	projected area of the imprint
ABS-ZnO	acrylonitrile-butadiene-styrene–zinc oxide nanocomposite
AM	additive manufacturing
β	geometry factor of the indenter
C	creep increment
c_r	creep rate
DMA	dynamic mechanical analyzer
DSI	depth-sensing indentation
E_r	reduced indentation modulus of elasticity
F	load force
F_{max}	maximum load force
FDM	fused deposition modeling
H	hardness
Δh	change in depth
h	indentation depth
h_0	indentation depth at the end of the cycle
h_1	pre-creep indentation
h_2	indentation depth at the end of the load phase
h_{max}	maximum indentation depth
n	number of cycles
PLA	polylactic acid
R	relaxation increment
RT	rapid tooling
S	the initial slope of the unload curve
SLA	stereolithography
SLS	selective laser sintering
T_g	glass transition temperature range
Δt	change in time
t_{creep}	time of the creeping phase
t_{h1}	time instant at h_1 indentation depth
t_{heat}	time of the heating phase
t_{hmax}	time instant at
h_{max}	indentation depth
t_{rest}	time of the rest phase
v_{load}	loading rate
v_{unload}	unloading rate

injection molding tool inserts, additional tests are needed. Palmer and Colton [19] carried out a detailed study on the geometric parameters and failure mechanism of inserts manufactured by SLA. Bagalkot et al. [20] and Surace et al. [21] examined surface degradation modes and identified possible causes. Krizsma et al. [22] used a new method for in-situ monitoring of inserts. Colton and LeBaut [23] examined the effects of heat on SLA injection mold inserts, and found that the degree of cure of the inserts increased with the number of shots, and the ejection force decreased. Rodet and Colton [24] carried out a comprehensive study on the failure of rapid prototyping inserts. The results show that the most significant degradation occurs on the surface. Yet surface properties are rarely investigated.

In most cases, the hardness of materials was tested. The depth sensing indentation (DSI) test is an excellent way to measure surface mechanical properties [25–29] and indentation creep [30], and test crack propagation [31–33]. This technique is also well suited for cyclic tests [34–37]. The hardness and indentation test is also ideally suited to test samples with treated surfaces [38,39]. Based on these results, this method would also be suitable for determining the surface mechanical properties of injection molding tool inserts. The DSI test allows for a diverse mechanical characterization of the tested material. Its advantage over the hardness test is that it can measure several mechanical properties, and instead of optical examination, indentation depth is considered. During the test, the computer-controlled testing equipment presses the indenter at a constant indentation speed into the surface and then lifts it at the same rate. The machine continuously measures the load force (F) as a function of indentation depth (h) and produces the so-called indentation F-h curve [25,26].

Our previous paper [40] presented our new clamp, which we designed for a dynamic mechanical analyzer (DMA) It allows indentation tests with different indenters in the device. DMA uses sinusoidal loading under continuously varying temperatures to determine the viscoelastic parameters of the tested material. In this way, information can be obtained about the transition phases of the material and the limits of operational temperature. Static or cyclic indentation tests can be performed in a wide range of temperatures with the equipment. This paper presents the results of cyclic tests on photopolymer test specimens manufactured with the PolyJet technology. This material (VeroWhite Plus) is widely used by researchers as a material for small series production of injection molding tool inserts with the use of additive manufacturing techniques [19,22]. The cyclic measurement program was set to simulate the injection molding cycle.

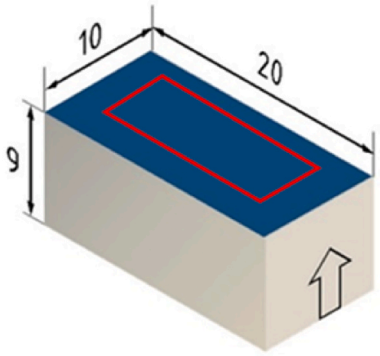

Fig. 1. Test specimen geometry produced by PolyJet technology – the direction of construction is indicated by the arrow.

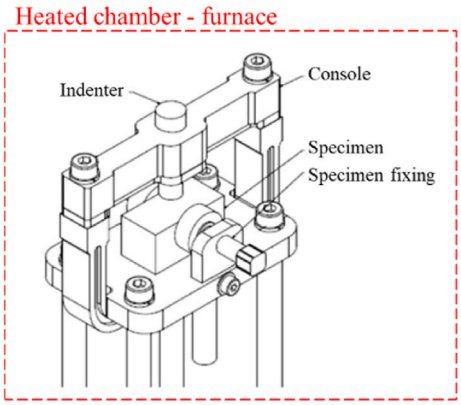

Fig. 2. The indentation clamp in TA DMA Q800.

2. Experimental

2.1. Investigated material

For the tests, we used an epoxy-based photopolymer, type VeroWhite Plus (Stratasys, RGD835), and an Alaris 30 PolyJet (Objet Geometries

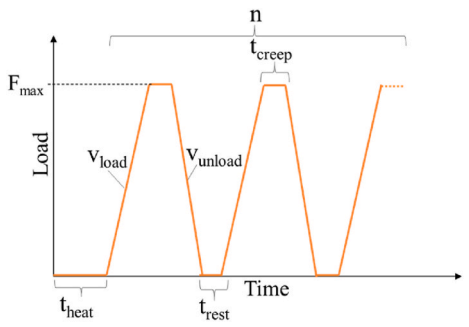

Fig. 3. The test program of the cyclic indentation test.

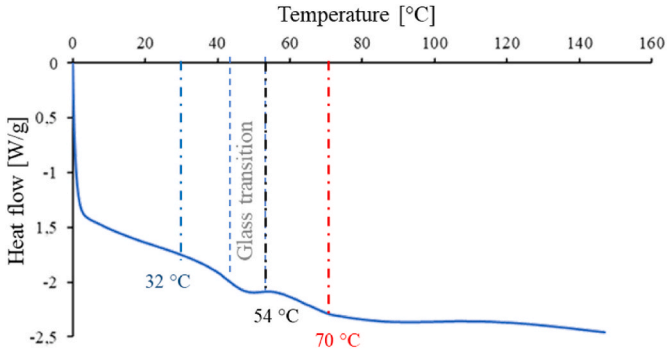

Fig. 4. DSC curve of the tested material, marked with the test temperatures (32 °C, 54 °C, 70 °C).

Ltd., Israel) device to fabricate the 9 × 10 × 20 mm rectangular test specimens in glossy mode. Tests were performed on the surface marked in blue, inside the red area in Fig. 1, perpendicular to the direction of construction, on the top of the specimen. During production, the specimens are 100% cross-linked, but we waited an additional week before the tests to allow time for any parts not cross-linked yet to cross-link. Until then, the test specimens were stored in a 50% humidity desiccator.

2.2. Experimental methods

We used the clamp we designed (Fig. 2) in a TA Q800 DMA (TA Instruments, USA) with a Vickers indenter to perform the indentation tests. Before the tests, the clamp was calibrated with the software of the DMA, to filter out the compliance of the equipment. Before each test, the zero point was recorded on the specimens. The indenter touches the sample surface and, with the application of a minimum force, picks up the initial point, releases the load, and starts the measurement program.

The test program is shown in Fig. 3. We wanted the program to follow a typical injection molding cycle, so we maintained the maximum load for 30 s, simulating the injection molding phase and a resting phase of 30 s after unloading, simulating ejection and the phase before the next cycle. The number of cycles (n) is set to 50. Uploading and unloading were set to a uniform 30 N/min, with a maximum load force (F_{max}) of 18 N. The minimum force was 0,001 N, therefore the contact between the specimen and the indenter did not cease. The test was carried out 5 times at each temperature level.

The thermal transitions are shown on the DSC curve of the material (Fig. 4), and the temperature levels for our measurements were determined on this basis. Tests were carried out at three temperatures, 32 °C, 54 °C, and 70 °C. Our aim was to analyze the effect of the test temperature at room temperature, the glass transition temperature and a higher temperature point. The heating rate was 3 °C/min. After warming up, a heating time of 3 min was applied before the cycles to allow the outer layers to warm up.

3. Results and discussion

The results of tests at different temperatures are shown in Fig. 5. The graphs clearly show that significant changes occur with increasing temperature. When the temperature was increased, the indentation depth and its amplitude also increased (Fig. 5/a). As the cycle progresses, some increase is expected theoretically, which is also seen in the tests at 32 °C, but the indentation curves (Fig. 5/b) are shifted to higher temperatures. Examining the force-displacement curves, we found that as the cycles progressed, hysteresis decreased and then became nearly constant. This phenomenon can be paralleled with the Mullins effect studied in detail in rubbers [41] and semicrystalline polymers [42]. The gradual change in hysteresis is influenced by the delayed elastic and the residual deformation components, and the plastic deformation due to the sharp geometry of the Vickers indenter, which already occurs during initial contact [43]. Due to both plastic and residual deformation, the starting point of each cycle is shifted towards positive values.

In the case of the hysteresis curves (Fig. 6), a steady state of

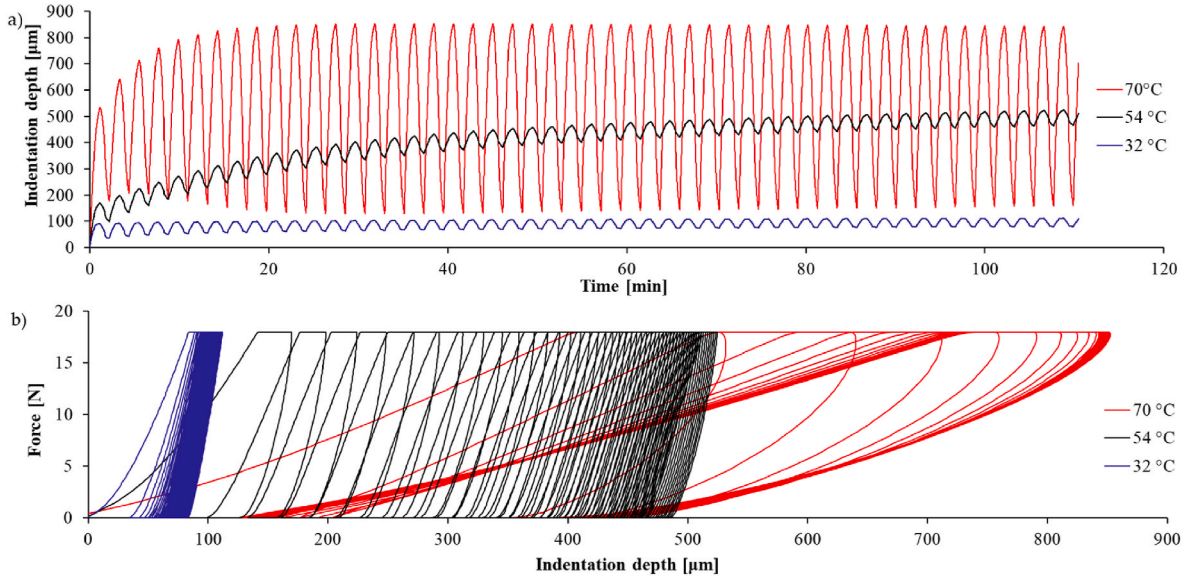

Fig. 5. Indentation depth versus time (a) and indentation curves (b) at the temperatures investigated.

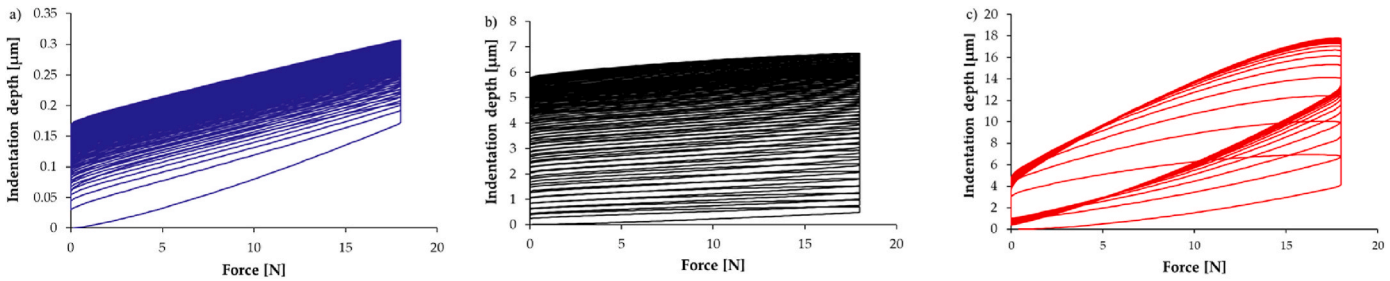

Fig. 6. Hysteresis curves at 32 °C (a), 54 °C (b) and 70 °C (c).

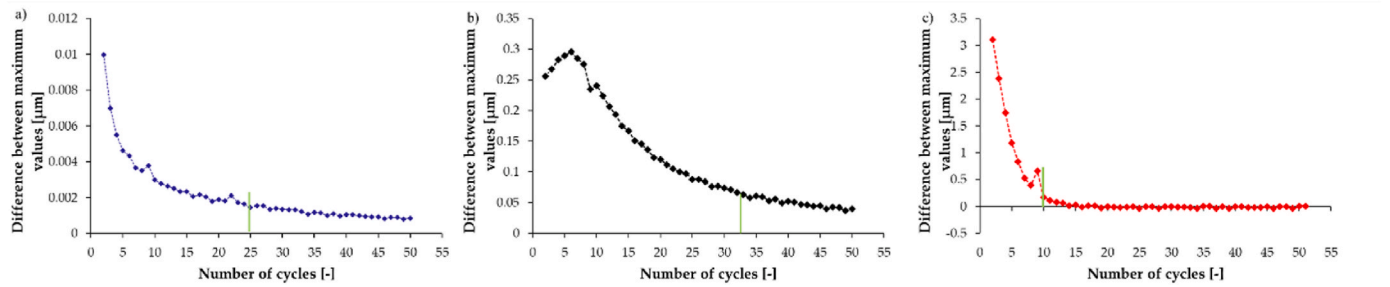

Fig. 7. Differences between the maximum values at 32 °C (a), 54 °C (b) and 70 °C (c).

hysteresis can be seen for tests at 70 °C, even at low cycle rates. This is certainly related to the fact that the material is already in a highly elastic state at this temperature.

Hysteresis stabilizes after a different number of cycles at different temperatures. To investigate this, we examined the difference in the maximum values obtained in each cycle and plotted it as a function of cycle number (Fig. 7), except for the first cycle in each case, for better representation. For tests at 32 °C, the difference is negligible from cycle 25 onwards (less than 1% of the change compared to the first cycle), but at 70 °C, it is already true after the 10th cycle. However, for the glass transition range, this is only observed between cycles 30 and 35.

Smerdova et al. [35], got similar results in an earlier study. They investigated three materials: an amorphous, a partially crystalline and a thermosetting polymer. For all three, they observed the appearance of hysteresis and a decrease in hysteresis as the cycles progressed. Still, they found a significantly larger shift in hysteresis for partially crystalline HDPE. The amorphous phase of HDPE is in a rubbery state at room temperature. By increasing the temperature to 70 °C, we found that our test material softened and reached a rubbery state. At this level, we observed a more significant shift between hysteresis in the first ten cycles than at lower temperatures.

Moreover in their measurements on HDPE, they also tested three different cycle times. The longer cycle time and the increased temperature gave similar results, i.e., the indentation depth increased in both cases. Based on this experience, it may be worthwhile to conduct further experiments to improve cyclic indentation test further and to help explore the relationship between temperature dependence and test speed.

The unloading section of the indentation curves can be used to determine the indentation elastic modulus. The depth of indentation starts to decrease at the basis of the curve. It usually starts as soon as the loading force is reduced. However, in some cases, usually at low loading rates or when the loading force is too high, the curves may show a “nose effect”. This makes it difficult to evaluate the results, especially the contact area and the parameters that can be calculated from it (indentation elastic modulus, contact stiffness). To correct this, researchers maintain the maximum load for a short period before loading [44]. As shown in Fig. 5/b, increasing temperature can also cause this effect, and it is more significant when the temperature is higher. Further

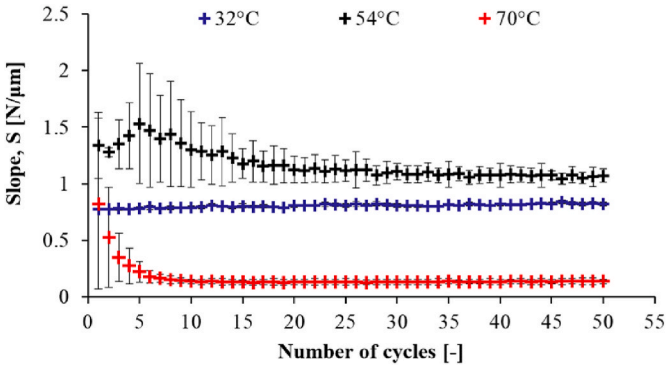

Fig. 8. Initial slope of the unloading curves as a function of the number of cycles.

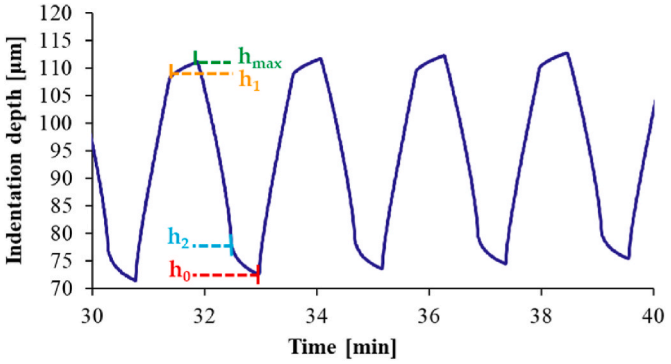

Fig. 9. Notable points of the indentation depth–time curve, marked on the highlighted part of the measured curve at 32 °C.

experiments should be carried out, which would show how this can be avoided at higher temperatures (possibly with even longer holding times) or if it cannot be compensated for due to the plastic behavior of the material.

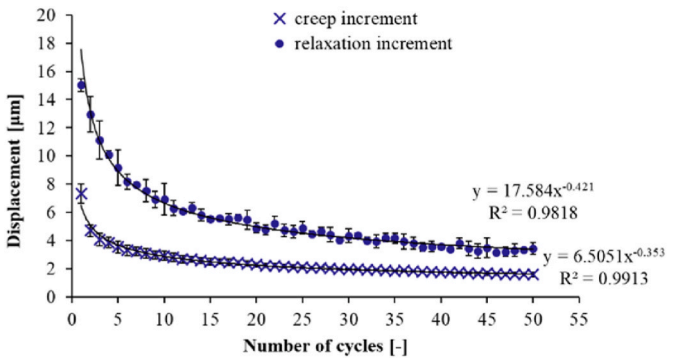

Fig. 10. Creep and relaxation increments as a function of cycle number for tests at 32 °C.

Examining the slope of the tangent of the load curves (Fig. 8), we found that tests at 54 °C resulted in curves with a steeper slope than tests at 32 °C and 70 °C. This suggests that temperature does not have a clear effect on the slope of the curve or indentation depth. However, tests at 32 °C have a small variance and show a nearly linear, small increase with increasing cycle numbers, while at elevated temperatures, there are larger differences in hysteresis at the initial stage, but from cycle 15 onwards, both 54 °C and 70 °C tests show a pattern similar to the 32 °C tests.

Fig. 9 shows an enlarged part of the indentation depth–time curve. It shows that under a constant load force, deformation increases continuously with time, creep occurs, while in the unloaded, resting phase, the deformation reverts. To explore how creep and relaxation change during cyclic loading, we defined the creep increment ($C = h_{max}$-h_1) and relaxation increment ($R = h_2$-h_0) parameters and investigated their variation as a function of the number of cycles.

At 32 °C, both the creep and relaxation increments decrease gradually, and for both sets of points, a power-law trend line can be fitted with high accuracy (Fig. 10). While for relaxation, standard deviation was more significant in the first few cycles—it also gradually decreases—for creep, it remained small throughout. Also, the rate of relaxation is greater than creep rate, but as the number of cycles increases, the difference between them gradually decreases, which will be discussed later.

Test results at 54 °C had higher standard deviation—this temperature is the glass transition temperature (T_g) of the material (Fig. 11/a). An initial decrease followed by an increase and a further reduction in the change in deformation was observed. A power-law trend line was fitted from cycle 15 onwards (Fig. 11/b). The cause of this behavior is the glass transition temperature range, and these tests should be repeated on other materials. It is a future task, and it will show the behavior of the material around T_g, taking into account the limits of the DMA (e.g., the temperature stability of the equipment in isothermal mode ±0.1 °C) and the time required for the outer layers of the test specimen to reheat.

No clear trend can be determined for tests at 70 °C (Fig. 12), but after the initial 5–10 cycles, there is a nearly linear phase, in line with Fig. 4/b. Standard deviation is significantly lower than that of the test results at 54 °C, and the higher values can be attributed to the initial cycles.

We also calculated the creep rate (c_r) during each cycle in the creep phase, which can be calculated with the following equation:

$$c_r = \frac{\Delta h}{\Delta t} = \frac{h_{max} - h_1}{t_{h_{max}} - t_{h_1}}, \quad (1)$$

where h_1 is indentation at maximum load, t_{h1} is the corresponding time instant, h_{max} is the indentation at the end of the creeping stage, and t_{hmax} is the related time instant. The same series of points were obtained for the creep increment as expected (Fig. 13). In tests at 32 °C and 54 °C, the creep rate decreased, in contrast to the results at 72 °C, where a decrease follows an initial increase. As the temperature increases, the creep rate increases. The creep rate calculated from the 70 °C results is 14 times higher in the initial stage and 47 times higher in the 50th cycle than the creep rate at 32 °C.

Examining the change in indentation depth in the uploading and unloading phases (Fig. 14), we find that the values in both phases decrease gradually, but their ratio increases with the number of cycles. Of course, residual deformation will never be zero, since plastic deformation prevents this, but elastic deformation also plays an important role during the cycles. In the first 5 to 10 cycles, recovery is incomplete, but as the deformation rate decreases, approaching the limit, recovery is close to 100%.

Estimates for more cycles can be reliably made from the results of the tests at room temperature. In our preliminary tests, we found a fit of over 95% for five cycles, but this increased further as the number of cycles was increased. We also examined the development of the accuracy of the

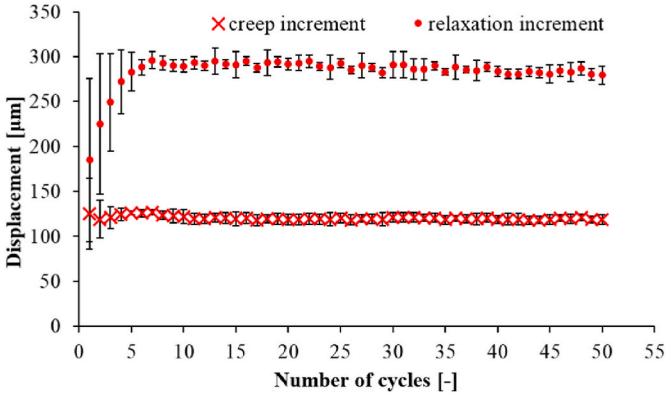

Fig. 12. Creep and relaxation curves as a function of cycle number for tests at 70 °C.

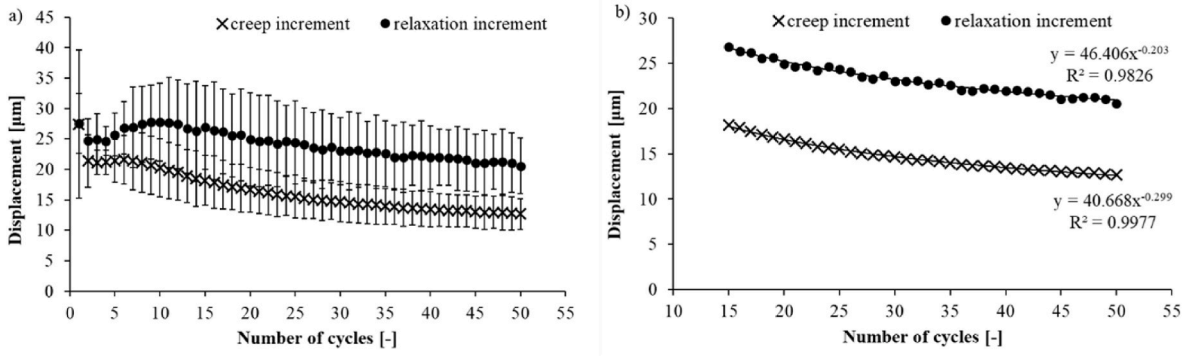

Fig. 11. Creep and relaxation increments as a function of cycle number for tests at 54 °C (a) and the highlighted points after the 15th cycle (b).

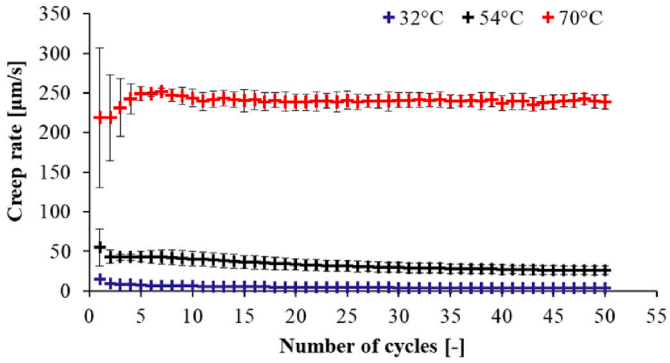

Fig. 13. The creep rate at different temperatures as a function of cycles.

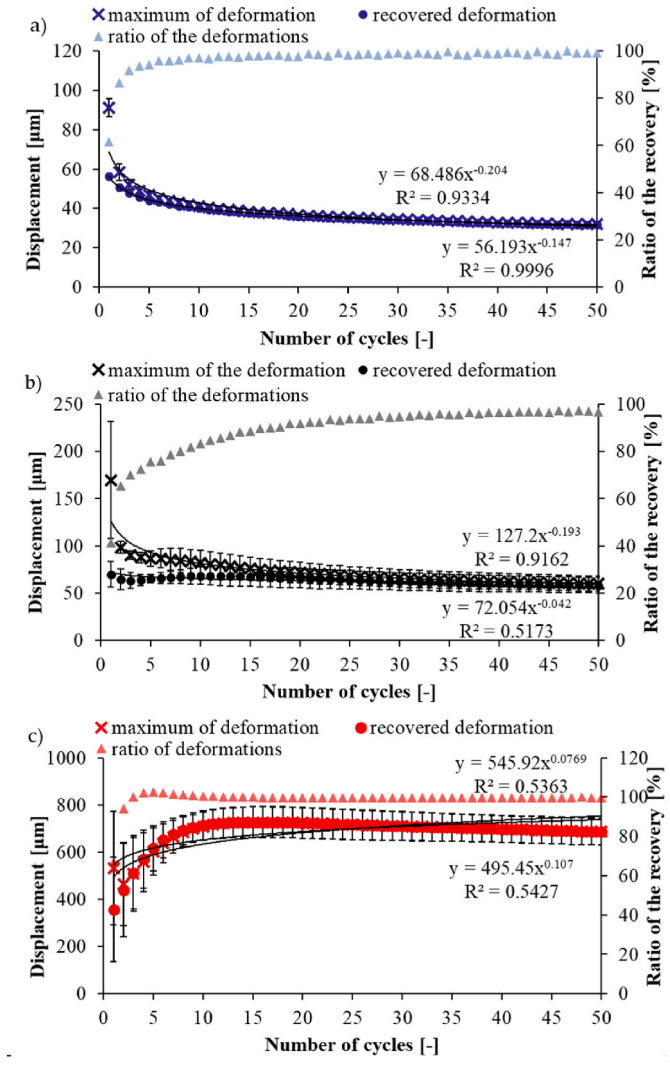

Fig. 14. Displacement during loading and recovery during unloading and their ratio at 32 °C (a), 54 °C (b), and 70 °C (c).

fit for 10, 20, 30 and 40 cycles. If we take a 98% fit as the limit, 30 cycles may be sufficient for the creep increment and relaxation of the given material (Table 1). It is significant because a 50-cycle test takes ~110 min, whereas 30 cycles can be performed in ~65 min. However, we think it is worthwhile to complete a 1000-cycle test and investigate the accuracy of the power-law approximation to estimate material behavior. In 1000 cycles, long-term properties can be analyzed. In this case, it is worth combining the indentation tests with optical tests. Our aim is to develop a procedure, based on the proven master curve construction method for creep tests, which can also help to understand the long-term behavior of the material by means of cyclic tests.

Table 1
Parameters of the $y = ax^b$ power functions fitted to the creep and relaxation increment values of cyclical tests at 32 °C.

	Creep increment			Relaxation increment		
n	*a*	*b*	Fitting accuracy (R^2)	a	b	Fitting accuracy (R^2)
5	15.418	0.306	98.11	6.9304	0.441	95.77
10	15.968	0.359	98.22	6.6	0.372	96.22
20	16.377	0.372	98.51	6.385	0.343	97.76
30	16.667	0.383	98.52	6.3891	0.344	98.62
40	17.081	0.394	98.42	6.4326	0.346	98.98
50	17.584	0.407	98.15	6.5051	0.353	99.13

We used the results of tests at different temperatures to investigate the indentation elastic modulus and hardness in each cycle. The reduced indentation modulus of elasticity (E_r, [MPa]) of the specimen can be determined [25]:

$$E_r = \frac{1}{\beta} \bullet \frac{\sqrt{\pi}}{2} \bullet \frac{S}{\sqrt{A}}, \tag{2}$$

where A [µm^2] is the projected area of the imprint at the maximum indentation depth (h_{max}). This is a calculated value, entered as shown in the denominator of equation (3). β is a geometry factor of the indenter, and S is the initial slope of the unload curve. Hardness can be calculated in a similarly simple way [25]:

$$H = \frac{F}{A} = \frac{F_{max}}{24.5 \bullet h_{max}^2}, \tag{3}$$

where 24.5 is a constant for a Vickers probe and h_{max} is the maximum indentation depth achieved in each cycle.

Fig. 15 shows the results, both the indentation elastic modulus and hardness. We observed a decrease at all temperatures, which is in line with the results found in the literature. In addition, both elastic modulus and hardness also decrease as cycle number increases. At 32 °C and 54 °C, a power-law trend can be fitted to these points with an R^2 above 96%, but fitting accuracy dramatically decreases at 70 °C. The indentation elastic modulus (Fig. 11/a) decreases much more in tests performed at 54 °C than in tests at 32 °C. Standard deviation is nearly constant at 32 °C, and at 54 °C and 70 °C. It is significant for the first ten cycles, then gradually decreases until it is negligible. As cycle number increases, hardness decreases, but it also reaches a specific limit, and the rate of decrease gradually slows down.

4. Conclusions

In this article, we investigated the material (VeroWhite Plus) of injection molding tool inserts produced by additive manufacturing. Polymer mold inserts are characterized by a high incidence of surface defects, as shown in the literature. It is important to investigate surface mechanical properties, for which the ideal method is the depth-sensing indentation test. This article aimed to examine material behavior under cyclic loading, which models consecutive injection molding cycles. For this purpose, we performed tests in a DMA with high accuracy at three temperatures using the indentation clamp we designed. The tests at 32 °C show that indentation depth gradually increased as the number of cycles increased, while the creep rate showed a decreasing trend. The values of the tested mechanical properties decreased.

The results showed that the method is well suited for exploring temperature dependence. The material softened as temperature increased. Its deformability rose. Standard deviation was very high in the glass temperature range, at 54 °C, and in the first 15 cycles, material

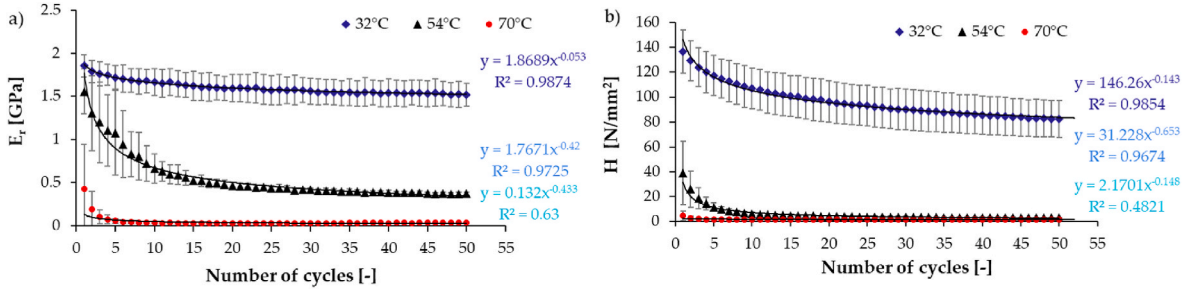

Fig. 15. Changing of the reduced indentation elastic modulus (a) and hardness (b) as a function of cycle number at 32 °C, 54 °C, and 70 °C.

behavior was difficult to analyze. At 70 °C, the material became soft, and the change in creep rate was the opposite of what had been observed at lower temperatures. The insert can be subjected to considerably higher heat loads, as the melting temperature of the material of the injection molded product can be above 100 °C. In the future, it is worthwhile to investigate thermal stresses in more detail, perform the above-mentioned cyclical tests at several temperature points, and analyze the effect of heating time as well.

The steady state of the hysteresis can be observed after a different number of cycles at different temperatures. The earliest time of the steady state is after the 10th cycle when measured at 70 °C, which may be due to the highly elastic state of the material. This phenomenon resembles the Mullins effect typical of rubbers.

Our results indicate that we can estimate deformation at 32 °C with high accuracy by fitting a power law. For this, performing tests in as few as 30 cycles is enough. However, we would like to extend our tests to a larger number of cycles (up to 1000 cycles) to investigate what other material behavior may occur with more extended tests. We also consider it worthwhile to combine the tests with optical examination to check for visible damage (e.g., cracks) around the impression.

Author statement

Luca Kotrocz: Conceptualization, Data curation, Writing- Original draft preparation, **Péter Bakonyi:** Writing - Review & Editing.

Declaration of competing interest

The authors declare that they have no known competing financial interests or personal relationships that could have appeared to influence the work reported in this paper.

Data availability

Data will be made available on request.

Acknowledgements

This work was supported by the National Research, Development and Innovation Office, Hungary (2019–1.1.1-PIACI-KFI-2019-00205, 2018–1.3.1-VKE-2018-00001, OTKA FK134336). The research reported in this paper and carried out at BME has been supported by the NRDI Fund (TKP2020 IES, Grant No. BME-IE-NAT) based on the charter of bolster issued by the NRDI Office under the auspices of the Ministry for Innovation and Technology.

References

[1] N.P. Karapatis, J.P.S. van Griethuysen, R. Glardon, Direct rapid tooling: a review of current research, Rapid Prototyp. J. 4 (1998) 77–89, https://doi.org/10.1108/13552549810210248.
[2] A.Y.C. Nee (Ed.), Handbook of Manufacturing Engineering and Technology, Springer London, London, 2015, https://doi.org/10.1007/978-1-4471-4670-4.
[3] J.G. Kovács, F. Szabó, N.K. Kovács, A. Suplicz, B. Zink, T. Tábi, H. Hargitai, Thermal simulations and measurements for rapid tool inserts in injection molding applications, Appl. Therm. Eng. 85 (2015) 44–51, https://doi.org/10.1016/j.applthermaleng.2015.03.075.
[4] D.V. Rosato, D.V. Rosato, M.G. Rosato (Eds.), Injection Molding Handbook, Springer US, Boston, MA, 2000, https://doi.org/10.1007/978-1-4615-4597-2.
[5] W. Grellmann, S. Seidler (Eds.), Polymer Testing, second ed., Hanser Publishers, Munich, 2013.
[6] M. Galeja, A. Hejna, P. Kosmela, A. Kulawik, Static and dynamic mechanical properties of 3D printed ABS as a function of raster angle, Materials 13 (2020) 297, https://doi.org/10.3390/ma13020297.
[7] K. Szykiedans, W. Credo, Mechanical properties of FDM and SLA low-cost 3-D prints, Procedia Eng. 136 (2016) 257–262, https://doi.org/10.1016/j.proeng.2016.01.207.
[8] V.D. Sagias, K.I. Giannakopoulos, C. Stergiou, Mechanical properties of 3D printed polymer specimens, Procedia Struct. Integr. 10 (2018) 85–90, https://doi.org/10.1016/j.prostr.2018.09.013.
[9] D. Miedzińska, R. Gieleta, E. Małek, Experimental study of strength properties of SLA resins under low and high strain rates, Mech. Mater. 141 (2020), 103245, https://doi.org/10.1016/j.mechmat.2019.103245.
[10] N. Vidakis, M. Petousis, A. Maniadi, E. Koudoumas, G. Kenanakis, C. Romanitan, O. Tutunaru, M. Suchea, J. Kechagias, The mechanical and physical properties of 3D-printed materials composed of ABS-ZnO nanocomposites and ABS-ZnO microcomposites, Micromachines 11 (2020) 615, https://doi.org/10.3390/mi11060615.
[11] I. Anderson, Mechanical properties of specimens 3D printed with virgin and recycled polylactic acid, 3D Print. Addit. Manuf. 4 (2017) 110–115, https://doi.org/10.1089/3dp.2016.0054.
[12] M.M. Hanon, R. Marczis, L. Zsidai, Influence of the 3D printing process settings on tensile strength of PLA and HT-PLA, Period. Polytech. - Mech. Eng. 65 (2020) 38–46, https://doi.org/10.3311/PPme.13683.
[13] C. Kundera, T. Kozior, Mechanical Properties of Models Prepared by SLS Technology, Bydgoszcz, Poland, 2018, 020012, https://doi.org/10.1063/1.5056275.
[14] A. Sá Ribeiro, N. Hopkinson, C. Henrique Ahrens, Thermal effects on stereolithography tools during injection moulding, Rapid Prototyp. J. 10 (2004) 176–180, https://doi.org/10.1108/13552540410538996.
[15] P. Gay, D. Blanco, F. Pelayo, A. Noriega, P. Fernández, Analysis of factors influencing the mechanical properties of flat PolyJet manufactured parts, Procedia Eng. 132 (2015) 70–77, https://doi.org/10.1016/j.proeng.2015.12.481.
[16] J.P. Moore, C.B. Williams, Fatigue properties of parts printed by PolyJet material jetting, Rapid Prototyp. J. 21 (2015) 675–685, https://doi.org/10.1108/RPJ-03-2014-0031.
[17] L. Dai, J. Song, S. Qu, R. Xiao, Triple-shape memory effect in 3D-printed polymers, Express Polym. Lett. 14 (2020) 1116–1126, https://doi.org/10.3144/expresspolymlett.2020.91.
[18] W. Shan, H. Zhong, H. Mo, S. Zhao, P. Liu, Epoxy acrylate-based shape memory polymer via 3D printing, Express Polym. Lett. 15 (2021) 1126–1134, https://doi.org/10.3144/expresspolymlett.2021.91.
[19] A. Palmer, J. Colton, Failure mechanisms in stereolithography injection molding tooling, Polym. Eng. Sci. 40 (2000) 1395–1404, https://doi.org/10.1002/pen.11269.
[20] A. Bagalkot, D. Pons, D. Symons, D. Clucas, Categorization of failures in polymer rapid tools used for injection molding, Processes 7 (2019) 17, https://doi.org/10.3390/pr7010017.
[21] R. Surace, V. Basile, V. Bellantone, F. Modica, I. Fassi, Micro injection molding of thin cavities using stereolithography for mold fabrication, Polymers 13 (2021) 1848, https://doi.org/10.3390/polym13111848.
[22] Sz Krizsma, N.K. Kovács, J.G. Kovács, A. Suplicz, In-situ monitoring of deformation in rapid prototyped injection molds, Addit. Manuf. 42 (2021), 102001, https://doi.org/10.1016/j.addma.2021.102001.
[23] J.S. Colton, Y. LeBaut, Thermal effect on stereolithography injection mold inserts, Polym. Eng. Sci. 40 (2000) 1360–1368, https://doi.org/10.1002/pen.11265.
[24] V. Rodet, J.S. Colton, Properties of rapid prototype injection mold tooling materials, Polym. Eng. Sci. 43 (2003) 125–138, https://doi.org/10.1002/pen.10011.
[25] W.C. Oliver, G.M. Pharr, An improved technique for determining hardness and elastic modulus using load and displacement sensing indentation experiments, J. Mater. Res. 7 (1992) 1564–1583, https://doi.org/10.1557/JMR.1992.1564.

[26] W.C. Oliver, G.M. Pharr, Measurement of hardness and elastic modulus by instrumented indentation: advances in understanding and refinements to methodology, J. Mater. Res. 19 (2004) 3–20, https://doi.org/10.1557/jmr.2004.19.1.3.
[27] S. Arunkumar, A review of indentation theory, Mater. Today Proc. 5 (2018) 23664–23673, https://doi.org/10.1016/j.matpr.2018.10.156.
[28] J. Sun, L.F. Francis, W.W. Gerberich, Mechanical properties of polymer-ceramic nanocomposite coatings by depth-sensing indentation, Polym. Eng. Sci. 45 (2005) 207–216.
[29] C. Brutti, A theoretical model for elastic-perfectly plastic flat cylindrical punch indentation, Mech. Mater. 155 (2021), 103770, https://doi.org/10.1016/j.mechmat.2021.103770.
[30] F. Quadrini, E.A. Squeo, A. Guglielmotti, Indentation creep of polymers. I. Experimental, Polym. Eng. Sci. 50 (2010) 2431–2439, https://doi.org/10.1002/pen.21602.
[31] S.R. Choi, J.A. Salem, Fracture toughness of PMMA as measured with indentation cracks, J. Mater. Res. 8 (1993) 3210–3217, https://doi.org/10.1557/JMR.1993.3210.
[32] X. Zhang, Z. Sun, X. Hu, Low temperature fracture toughness of PMMA and crack-tip conditions under flat-tipped cylindrical indenter, Polym. Test. 38 (2014) 57–63, https://doi.org/10.1016/j.polymertesting.2014.06.009.
[33] R. Růžek, J. Pavlas, R. Doubrava, Application of indentation as a retardation mechanism for fatigue crack growth, Int. J. Fatig. 37 (2012) 92–99, https://doi.org/10.1016/j.ijfatigue.2011.09.012.
[34] X. Li, B. Bhushan, A review of nanoindentation continuous stiffness measurement technique and its applications, Mater. Char. 48 (2002) 11–36, https://doi.org/10.1016/S1044-5803(02)00192-4.
[35] O. Smerdova, M. Pecora, M. Gigliotti, Cyclic indentation of polymers: instantaneous elastic modulus from reloading, energy analysis, and cyclic creep, J. Mater. Res. 34 (2019) 3688–3698, https://doi.org/10.1557/jmr.2019.289.
[36] B. Blinn, D. Görzen, M. Klein, D. Eifler, T. Beck, PhyBaLCHT – influence of indentation force on the results of cyclic hardness tests and investigations of comparability to uniaxial fatigue loading, Int. J. Fatig. 119 (2019) 78–88, https://doi.org/10.1016/j.ijfatigue.2018.09.025.
[37] H. Zhang, T. Lu, Q. Zhang, Y. Zhou, H. Zhu, J. Harms, X. Yang, M. Wan, M. F. Insana, Solutions to ramp-hold dynamic oscillation indentation tests for assessing the viscoelasticity of hydrogel by Kelvin-Voigt fractional derivative modeling, Mech. Mater. 148 (2020), 103431, https://doi.org/10.1016/j.mechmat.2020.103431.
[38] M. Benaissa, F. Benkhenafou, A. Ziadi, L.B.P. Martinez, F.J. Belzunce, L. Douadji, The effects of shot peening on the surface characteristics of 35NCD16 alloy steel, Period. Polytech. - Mech. Eng. 64 (2020) 199–206, https://doi.org/10.3311/PPme.13229.
[39] D. Kovács, J. Dobránszky, Effects of thermochemical surface treatments on the industrially important properties of X2CrNiMo 17-12-2 austenitic stainless steel, Period. Polytech. - Mech. Eng. 63 (2019) 214–219, https://doi.org/10.3311/PPme.13921.
[40] L. Kotrocz, P. Bakonyi, Pinpoint loading examinations of poly(lactic acid) biopolymers, Acta Technica Jaurinensis (2018) 206–217.
[41] J. Diani, B. Fayolle, P. Gilormini, A review on the Mullins effect, Eur. Polym. J. 45 (2009) 601–612, https://doi.org/10.1016/j.eurpolymj.2008.11.017.
[42] A.D. Drozdov, Mullins' effect in semicrystalline polymers, Int. J. Solid Struct. 46 (2009) 3336–3345, https://doi.org/10.1016/j.ijsolstr.2009.05.001.
[43] M.L. Oyen, R.F. Cook, A practical guide for analysis of nanoindentation data, J. Mech. Behav. Biomed. Mater. 2 (2009) 396–407, https://doi.org/10.1016/j.jmbbm.2008.10.002.
[44] A.H.W. Ngan, B. Tang, Viscoelastic effects during unloading in depth-sensing indentation, J. Mater. Res. 17 (2002) 2604–2610, https://doi.org/10.1557/JMR.2002.0377.